

## Electron ionization cross sections in the Born approximation\*

Eugene J. McGuire

*Sandia Laboratories, Albuquerque, New Mexico 87115*

(Received 25 February 1977)

Using the generalized oscillator-strength formulation of the Born approximation, electron ionization cross sections were calculated for 20 elements with  $19 \leq Z \leq 54$ . For Kr and Xe, good agreement (30%) is found for the total ionization cross section above 300 eV. Comparison with measured cross sections for producing various charge states in Kr and Xe showed significant discrepancies, which arise from neglect of configuration interaction. Comparison with measured total cross sections for other elements show limited agreement, though the agreement improves as one goes to higher  $Z$ .

### I. INTRODUCTION

Several years ago, I presented results<sup>1</sup> on electron and proton ionization calculations in the Born approximation via the generalized oscillator-strength formalism. In addition, I indicated<sup>2</sup> that scaling laws could be obtained for the cross section for ionization of atomic subshells. Since that time, two alternative calculational procedures have been used, the independent-particle-model (IPM) approach of Green and colleagues,<sup>3</sup> and the calculations of Omidvar, Kyle, and Sullivan<sup>4</sup> using a hydrogenic continuum orbital. The former set of calculations are largely limited to atmospheric gases, while the latter is limited by the use of the hydrogenic orbital. Manson<sup>5</sup> has performed calculations similar to mine, but for He and Al only. Earlier, I did not continue the calculations beyond  $Z=18$ , because (i) there was little data to compare with the calculations, and (ii) the calculations were time consuming on the computers then available. Reason (i) is still valid, and for the calculations reported approximately 6 hours of CDC-6600 time was used. The calculations were resumed because there is a need for electron ionization cross sections in various fusion programs, e.g., impurities in tokomaks, and pellet fusion via relativistic electron beams. For modeling these systems, scaled cross sections leading to temperature-dependent ionization rates are important. Thus, the calculations are motivated by the need for scaling laws, and to establish and verify the scaling laws, the generalized oscillator

strengths were calculated for 110 atomic subshells with  $18 \leq Z \leq 54$ . The scaled cross sections will be reported in the following paper.

Here I report total electron ionization cross sections and where possible compare them with available measurements. While the measurements are limited, some of the measurements form the basis of a widely used semiempirical cross section formula.<sup>6</sup> The systematic calculations reported here permit a critical discussion of the measurements.

The approach used is detailed in Sec. II, with some discussion of breakdown of the one-electron model and other sources of error. In Sec. III the calculations are compared with measurements on Kr and Xe; in Sec. IV, the alkalis and alkali earths; and in Sec. V, the column three elements, and Cu and Ag.

### II. CALCULATIONAL PROCEDURE

As in Ref. 1 the one-electron generalized oscillator strength (GOS) to the continuum per  $nl$  electron per  $\epsilon l'$  (continuum) hole is defined by

$$\frac{df_{nl}}{d\epsilon}(\epsilon, k^2, l') = \frac{\Delta E}{k^2} |\langle nl | e^{i\mathbf{k}\cdot\mathbf{r}} | \epsilon l' \rangle|^2, \quad (1)$$

where  $\Delta E = \epsilon - E_{nl}$  is in Ry (13.6 eV),  $-E_{nl}$  is the one-electron ionization energy of the  $nl$  subshell,  $\epsilon$  is the continuum electron energy, with  $\epsilon=0$  at the ionization threshold,  $r$  is in Bohr radii, and  $k$  in inverse Bohr radii, with  $df/d\epsilon$  in Ry<sup>-1</sup>. Expanding the exponential in Eq. (1) in terms of Legendre polynomials and Bessel functions leads to

$$\begin{aligned} \frac{k^2}{\Delta E} \frac{df_{n0}}{d\epsilon} &= (2l'+1) \left| \int_0^\infty j_l(kr) \varphi_{n0}(r) \varphi_{\epsilon l'}(r) dr \right|^2, \\ \frac{k^2}{\Delta E} \frac{df_{n1}}{d\epsilon} &= l' \left| \int_0^\infty j_{l'-1}(kr) \varphi_{n1}(r) \varphi_{\epsilon l'}(r) dr \right|^2 + (l'+1) \left| \int_0^\infty j_{l'+1}(kr) \varphi_{n1}(r) \varphi_{\epsilon l'}(r) dr \right|^2, \\ \frac{k^2}{\Delta E} \frac{df_{n2}}{d\epsilon} &= \frac{3}{2} \frac{l'(l'-1)}{(2l'-1)} \left| \int_0^\infty j_{l'-2}(kr) \varphi_{n2}(r) \varphi_{\epsilon l'}(r) dr \right|^2 + \frac{l'(l'+1)(2l'+1)}{(2l'+3)(2l'-1)} \left| \int_0^\infty j_{l'}(kr) \varphi_{n2}(r) \varphi_{\epsilon l'}(r) dr \right|^2 \\ &\quad + \frac{3}{2} \frac{(l'+1)(l'+2)}{(2l'+3)} \left| \int_0^\infty j_{l'+2}(kr) \varphi_{n2}(r) \varphi_{\epsilon l'}(r) dr \right|^2. \end{aligned} \quad (2)$$

The one-electron orbitals used in the calculation are discussed in Ref. 1. For  $19 \leq Z \leq 36$ , we approximated the quantity  $[-rV(r)]$  of Herman and Skillman<sup>7</sup> by a series of six straight lines, and for  $37 \leq Z \leq 54$ , by seven straight lines. The approximate potentials were those used in earlier photoionization calculations.<sup>8</sup> For convenience the calculations were done using  $k'$  and  $\epsilon'$  where  $k' = k(E_{nl})^{1/2}$  and  $\epsilon' = \epsilon/E_{nl}$ . The GOS were calculated on a  $20 \times 20$  grid of  $(k', \epsilon')$ , and summed up to  $l' = 12$ , when appropriate (as discussed in Ref. 1). The electron ionization cross section is given by<sup>9,10</sup>

$$\sigma = 4\pi(a_0)^2 \int_0^{\epsilon_{\max}} \frac{d\epsilon}{\epsilon + E_I} \times \int_{k_{\min}^2}^{k_{\max}^2} \sum_{l'=0}^{\infty} \frac{df_{nl}}{d\epsilon}(\epsilon, k^2, l') \frac{dk^2}{k^2},$$

where

$$\begin{aligned} \epsilon_{\max} &= \frac{1}{2}E_0, \\ k_{\max}^2 &= 2E_0 - \Delta E + 2[E_0(E_0 - \Delta E)]^{1/2}, \\ k_{\min}^2 &= 2E_0 - \Delta E - 2[E_0(E_0 - \Delta E)]^{1/2}, \end{aligned} \quad (3)$$

with  $E_0$  being the incident electron energy.

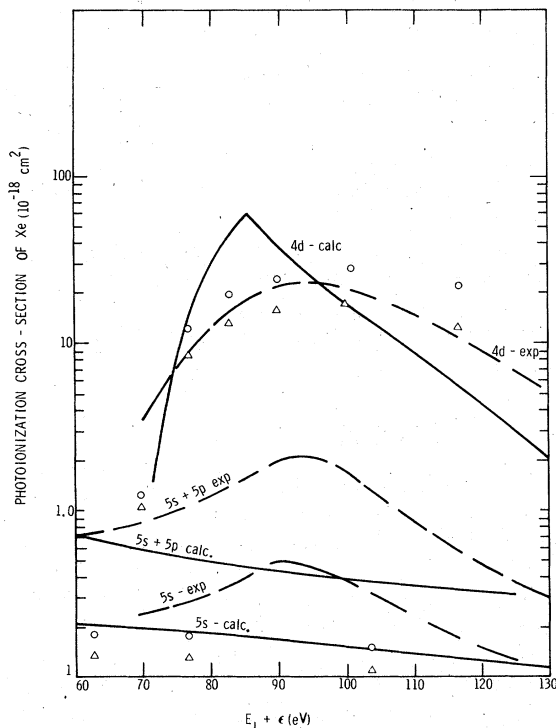


FIG. 1. Photoionization cross section of Xe between 60 and 130 eV. The solid lines are my calculations, the circles and triangles are the  $4d$  and  $5s$  HF results in dipole length and velocity formulations, respectively, from Ref. 12, while the dashed curves are measurements from Ref. 13.

In comparing the calculations with experimental total ionization cross sections, there are several possible sources of disagreement: (i) breakdown of the Born approximation, (ii) choice of central potential in the one-electron model, (iii) improper treatment of exchange, (iv) breakdown of the one-electron model, (v) neglect of inner-shell excitation followed by autoionization, and (vi) experimental inaccuracy.

(i) At low energy, the Born approximation is inaccurate. For the elements studied here, the total cross section is dominated by the cross section of the outermost two or three subshells. Low energy is then defined as energy less than four times the ionization potential of the innermost subshell contributing significantly to the total cross section.

(ii) I have shown<sup>11</sup> that the Born approximation excitation cross section for atomic oxygen, in a one-electron model, depends significantly on the choice of central potential. The scaling arguments developed elsewhere depend on ionization potentials, and when the ionization potential in the Herman-Skillman model differs from the experimental ionization potential, the calculated and measured subshell cross sections can differ. However, the hypothesis in the scaling arguments is that one can construct a scaled cross section from the calculations, then use the experimental ionization potential to calculate an improved subshell cross section.

(iii) Kennedy and Manson<sup>12</sup> have shown that the use of Hartree-Fock (HF), rather than Herman-Skillman (HS) wave functions, will considerably improve the agreement between calculated and experimental photoionization cross sections. One might expect a similar situation with electron ionization cross sections. However, since the Born approximation neglects exchange entirely, it seems inappropriate to include sophisticated exchange effects between ion-core and secondary electrons, and entirely neglect simple exchange between atom and primary electrons. At  $k^2 = 0$  the GOS is the optical oscillator, and in this limit one can calculate the subshell photoionization cross section. A comparison for Xe of my calculated subshell photoionization cross sections (solid curve), the experimental measurements of West *et al.*<sup>13</sup> (dashed curve), and the calculations of Kennedy and Manson (open circles and triangles), is shown in Fig. 1. The  $4d$  photoionization calculations of Kennedy and Manson are in reasonable agreement with the measurement, though there is a significant difference between the dipole length and dipole velocity calculation. However, for the  $5s$  photoionization cross section, the results of Kennedy and Manson do not significantly differ from my calculation; neither calculation showing the ob-

TABLE I. Electron ionization cross sections ( $10^{-16}$  cm<sup>2</sup>) for elements with  $19 \leq Z \leq 36$ .

$Z \backslash \epsilon$ (eV)	19	20	22	24	26	28	30	32	34	36
10	3.81	7.73	5.66	4.14	2.09	1.27	0.96	3.86	0.19	
11	4.00	8.47	6.49	4.76	2.75	2.03	1.40	4.83	1.18	
12	4.13	8.90	7.12	5.24	3.33	2.51	1.90	5.68	2.00	
13	4.20	9.20	7.59	5.60	3.81	2.95	2.38	6.43	3.28	0.004
14	4.24	9.38	7.83	5.86	4.17	3.34	2.73	7.08	4.26	0.35
15	4.30	9.41	8.05	6.07	4.45	3.62	3.05	7.48	5.42	0.98
20	4.22	9.03	8.19	6.44	5.08	4.34	3.93	9.21	9.59	3.71
25	4.39	8.26	7.82	6.43	5.14	4.46	4.23	9.85	11.8	5.67
30	5.01	7.47	7.32	6.21	4.99	4.40	4.28	9.92	13.0	6.86
40	5.75	6.17	6.38	5.74	4.53	4.05	4.09	9.37	13.7	7.97
50	5.95	5.29	5.59	5.28	4.08	3.70	3.80	8.61	13.3	8.19
60	5.91	4.59	5.02	4.93	3.68	3.35	3.51	7.90	12.7	8.06
100	5.78	3.14	3.61	3.61	2.73	2.49	2.72	5.79	9.98	6.74
200	4.99	1.86	2.27	2.34	1.83	1.68	1.86	3.57	6.29	4.41
300	4.17	1.34	1.69	1.76	1.43	1.29	1.46	2.66	4.68	3.31
400	3.57	1.04	1.35	1.43	1.18	1.06	1.22	2.16	3.77	2.69
600	2.77	0.73	0.97	1.06	0.89	0.80	0.92	1.59	2.76	1.98
800	2.28	0.56	0.76	0.85	0.71	0.64	0.74	1.28	2.19	1.59
1000	1.94	0.46	0.63	0.71	0.60	0.54	0.62	1.07	1.83	1.33
2000	1.13	0.239	0.349	0.400	0.339	0.304	0.357	0.60	1.03	0.76
3000	0.80	0.163	0.244	0.285	0.241	0.216	0.254	0.43	0.73	0.54
4000	0.63	0.124	0.189	0.223	0.189	0.169	0.199	0.336	0.57	0.43
6000	0.44	0.084	0.131	0.157	0.133	0.119	0.141	0.236	0.403	0.301
8000	0.343	0.064	0.102	0.122	0.103	0.092	0.110	0.184	0.313	0.235
10000	0.282	0.052	0.083	0.101	0.085	0.076	0.090	0.151	0.258	0.193

served peak at 90 eV.

(iv) The many-body calculations of Amusia *et al.*<sup>14</sup> reproduce the structure in the measured  $5s$  and  $(5s+5p)$  photoionization cross sections. This is an intershell interaction effect, and illustrates a significant breakdown in the one-electron approximation. An even more serious breakdown occurs for the  $4p$  subshell in Xe, as discussed by Gelius.<sup>15</sup> It is clear from Fig. 1 that at 60 and 130 eV, my calculated  $5s$  and  $(5s+5p)$  photoionization cross sections agree with the measurements. How serious an effect intershell interaction has on calculated electron total and subshell ionization cross sections is not immediately apparent from the photoionization results.

(v) In general, we assume inner-shell excitation is unimportant. If the penultimate subshell is excited, the resulting inner-shell vacancy can Auger decay leading to a singly charged ion. This would appear in the measurements as an enhancement of the outer-shell ionization cross section. In comparisons of calculation and experiment for neutrals, no evidence of significant enhancement is found.

(vi) In several of the comparisons of experiment and calculation, enhanced experimental cross sections are found at high energy. By considering and eliminating all processes which could contribute to

the enhancement, the conclusion is reached that the enhancement is likely to be an experimental artifact.

The calculated total cross sections ( $\sigma = \sum \sigma_{nl}$ ) are listed in Tables I and II. Cross sections are often measured via  $\sigma = \sum s_{nl} \sigma_{nl}$ , where  $s_{nl}$  is the number of electrons an ion has lost due to  $nl$  subshell ionization (i.e., the measurements use ion current). For cases where  $s_{nl} \neq 1$  is important the scaled subshell cross sections can be used to make the appropriate correction.

### III. KRYPTON AND XENON

Electron ionization in krypton and xenon has been measured in considerable detail. The calculated electron total ionization cross section for Kr and Xe, and three sets of measurements, are shown in Figs. 2 and 3. Above 1 keV, for clarity, the quantity  $E\sigma(E)$  is plotted. The measurements of Rapp and Englander-Golden<sup>16</sup> are lower than those of Asundi and Kurepa<sup>17</sup> at low energy, but are in good agreement with the measurements of Schram *et al.*<sup>18</sup> in the 0.6–1.0-keV range. The solid lines in Figs. 2 and 3 are total cross section calculations, i.e.,  $\sigma_{\text{tot}} = \sum_{nl} \sigma_{nl}$ . The dashed line is the cross section weighted by the final charge state of the ion. This is plotted because the experi-

TABLE II. Electron ionization cross sections ( $10^{-16} \text{ cm}^2$ ) for elements with  $37 \leq Z \leq 54$ .

$Z$	37	38	40	42	44	46	48	50	52	54
10	7.73	9.54	5.74	4.15	2.74	0.57	1.55	2.96	1.47	
11	7.83	10.3	6.69	4.88	3.13	1.01	2.20	3.87	2.39	0.54
12	7.83	10.6	7.42	5.53	3.45	1.35	2.80	4.69	3.53	1.84
13	7.76	10.9	8.01	5.84	3.77	1.71	3.25	5.44	4.74	2.60
14	7.69	10.9	8.34	6.18	3.95	2.00	3.62	6.24	5.75	3.97
15	7.59	11.0	8.64	6.46	4.16	2.28	3.92	6.89	6.69	4.83
20	6.84	10.4	9.15	7.18	4.69	3.31	4.70	9.09	9.94	8.89
25	7.01	9.44	9.05	7.45	4.88	3.95	4.94	10.0	11.8	11.2
30	6.69	8.52	8.73	7.54	4.93	4.39	5.00	10.3	12.6	12.5
40	6.34	7.21	8.06	7.51	4.96	4.95	4.85	9.88	12.5	13.4
50	5.95	6.34	7.41	7.50	5.00	5.28	4.70	9.15	11.6	12.9
60	5.60	5.67	6.88	7.28	5.07	5.52	4.59	8.53	10.7	12.0
100	4.43	4.17	5.40	6.29	4.88	5.73	4.44	7.16	8.38	9.33
200	2.78	2.48	3.44	4.34	3.64	4.53	3.52	4.95	5.58	6.20
300	2.02	1.75	2.53	3.29	2.83	3.58	2.78	3.78	4.21	4.68
400	1.60	1.36	2.02	2.66	2.32	2.96	2.36	3.08	3.41	3.78
600	1.13	0.94	1.45	1.94	1.72	2.22	1.78	2.28	2.51	2.77
800	0.88	0.72	1.15	1.54	1.38	1.80	1.43	1.82	2.00	2.21
1000	0.73	0.58	0.96	1.28	1.16	1.52	1.20	1.53	1.67	1.85
2000	0.395	0.302	0.53	0.72	0.67	0.88	0.69	0.87	0.94	1.04
3000	0.275	0.206	0.38	0.51	0.48	0.63	0.49	0.62	0.66	0.74
4000	0.212	0.156	0.293	0.40	0.38	0.50	0.39	0.49	0.52	0.58
6000	0.148	0.106	0.205	0.278	0.269	0.351	0.274	0.343	0.365	0.41
8000	0.113	0.081	0.159	0.216	0.210	0.275	0.214	0.268	0.284	0.32
10000	0.093	0.065	0.130	0.178	0.174	0.227	0.177	0.220	0.234	0.263

ments obtain  $\sigma_{\text{tot}}$  from ion current measurements, and assume singly charged ions. For Kr (Xe) the dashed curve is  $\sigma_{4p} + \sigma_{4s} + 2\sigma_{3d} + 3\sigma_{3p}$  ( $\sigma_{5p} + \sigma_{5s} + 2\sigma_{4d} + 3\sigma_{4p}$ ); the choice of final charge state is discussed later in this section. The contribution

from the inner  $p$  shell,  $3\sigma_{np}$ , is not more than 5% of the total at 10 keV. Between 0.3 and 10 keV my calculations agree with the Kr (Xe) measurements to 20% (30%), using either the cross section weighted or unweighted with the final charge state.

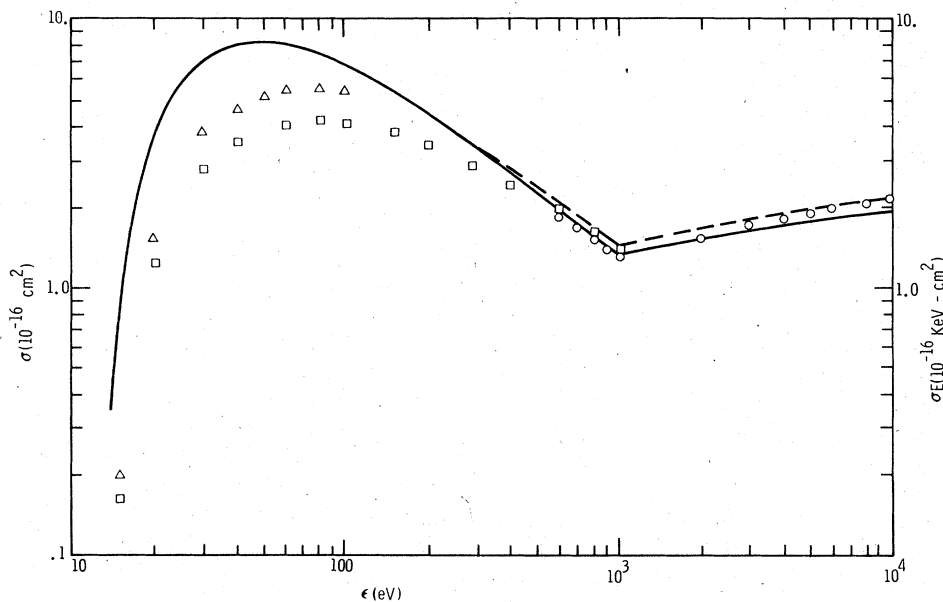


FIG. 2. Total electron ionization cross section of Kr. Above 1 keV,  $\sigma E$  vs  $E$  is plotted. The squares, triangles, and circles are from Refs. 16, 17, and 18, respectively. The solid curve is the sum of sub-shell cross sections, while the dashed curve is  $\sigma_{4p} + \sigma_{4s} + 2\sigma_{3d} + 3\sigma_{3p}$ .

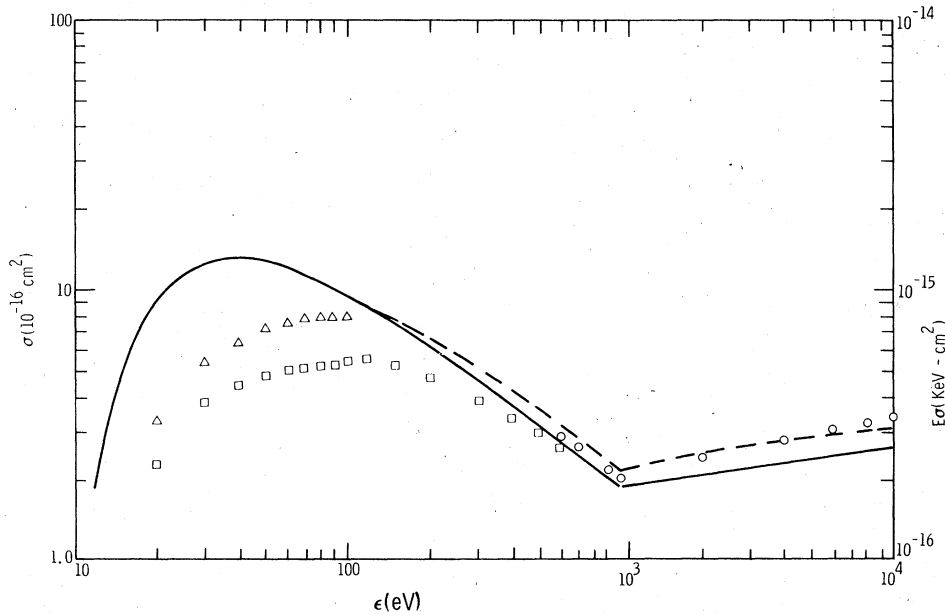


FIG. 3. Total electron ionization cross section of Xe. Above 1 keV,  $\sigma E$  vs  $E$  is plotted. The squares, triangles, and circles are from Refs. 16, 17, and 18, respectively. The solid curve is the sum of sub-shell cross sections, while the dashed curve is  $\sigma_{5p} + \sigma_{5s} + 2\sigma_{4d} + 3\sigma_{4p}$ .

However, while the calculated total cross sections are in good agreement with the measurements, the subshell cross sections show considerable variation. In Fig. 4, I compare the calculated Kr 4s and Xe 5s cross sections with the measurements of Luyken *et al.*<sup>19</sup> on a Bethe plot [ $E\sigma(E)$  vs  $E$ ]. The data are considerably lower in magnitude than the calculation, but comparable in slope (the dashed lines in Fig. 4 are the calculations normalized to the data at 10 keV). For a comparable discrepancy in Ar, Luyken *et al.* argue that there is a considerable configuration interaction between  $(3s)^1(3p)^6\ ^2S_{1/2}$  and  $(3s)^2(3p)^4(^1D)(3d)\ ^2S_{1/2}$ , and that this causes a reduction in the GOS, and a smaller cross section. Luyken *et al.* calculate the configuration mixing parameters for Ar, and show configuration interaction can bring the calculations into agreement with the measurement on Ar. This implies a second "3s" ionization threshold at an energy corresponding to  $(3p)^4\ ^1D(3d)\ ^2S_{1/2}$ . Then if "3s" GOS does not change significantly due to the change in thresholds (40.7 and 50.4 eV),<sup>20</sup> one might expect the "3s" cross section measured by counting singly charged ions to be larger than that measured by Luyken *et al.* in the  $(3s)^1(3p)^6 - (3s)^2(3p)^5$  transitions at 920 and 932 Å. It seems reasonable to expect a similar occurrence for 4s ionization in Kr and 5s ionization in Xe. However, one cannot separate singly charged ion production due to  $ns$  electron ionization from that due to  $np$  ionization.

El-Sherbini *et al.*<sup>21</sup> have measured cross sections for the production of various ion final states. I assume the measured cross section for producing

singly charged ions is  $\sigma_{4s} + \sigma_{4p}$  in Kr and  $\sigma_{5s} + \sigma_{5p}$  in Xe. A comparison of the measurements and calculations is shown in Fig. 5. The calculations and measurements differ by a factor of 2 but agree in slope.

A comparison of the ordinates in Figs. 4 and 5 indicate that outer  $s$ -shell ionization contributed no more than 10% of the total cross section for singly charged ions. Thus, there is a factor-of-2 discrepancy between the calculated and measured

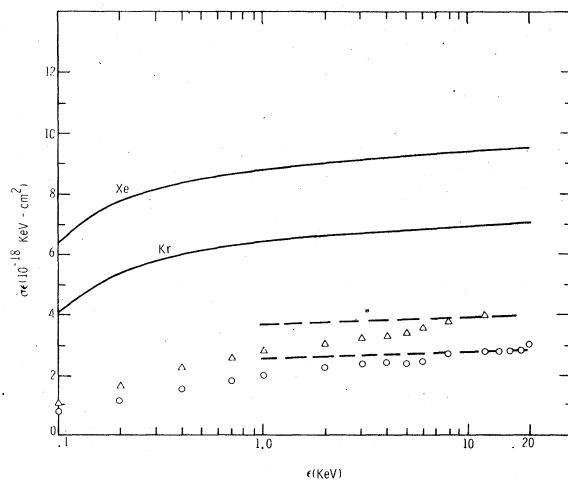


FIG. 4. Bethe plot of the 4s ionization cross section of Kr and the 5s ionization cross section of Xe. The circles (Kr) and triangles (Xe) are measurements from Ref. 19. The solid curves are the calculations, and the dashed lines are the calculations normalized to the measurements at 10 keV.

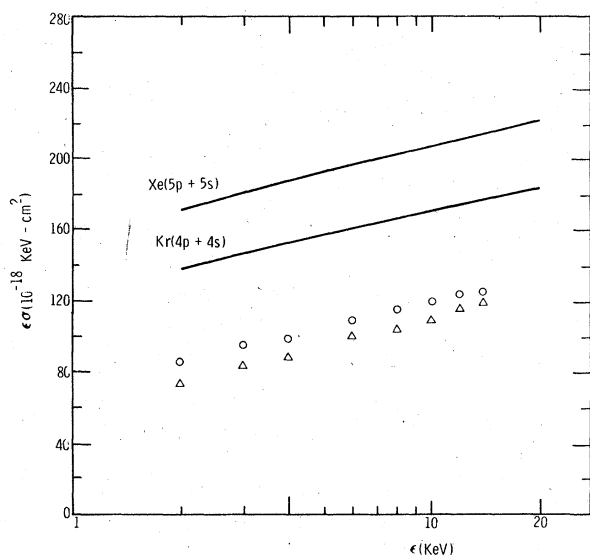


FIG. 5. Bethe plot of the ionization cross section for the two outermost subshells of Kr and Xe. The triangles (Kr) and circles (Xe) are measurements from Ref. 21 of the cross section for producing singly charged ions.

cross section for outer  $p$ -shell ionization; and yet the total cross sections are in reasonable agreement. Ten electrons in the outermost filled  $d$  shell should contribute significantly to the total cross section and should be the dominant source of doubly ionized ions. That is  $3d(4d)$  holes in Kr (Xe) will Auger decay to doubly charged ions. On the other hand,  $3p(4p)$  holes in Kr (Xe) will predom-

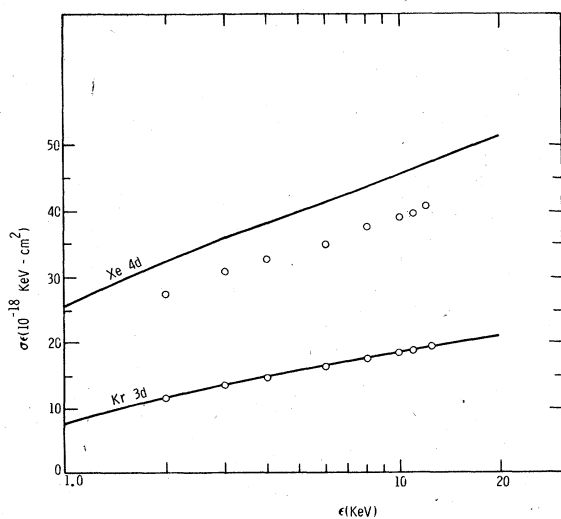


FIG. 6. Bethe plot of the ionization cross section for the outermost  $d$  shell of Kr and Xe. The circles are measurements from Ref. 21 of the cross section for producing only doubly charged ions.

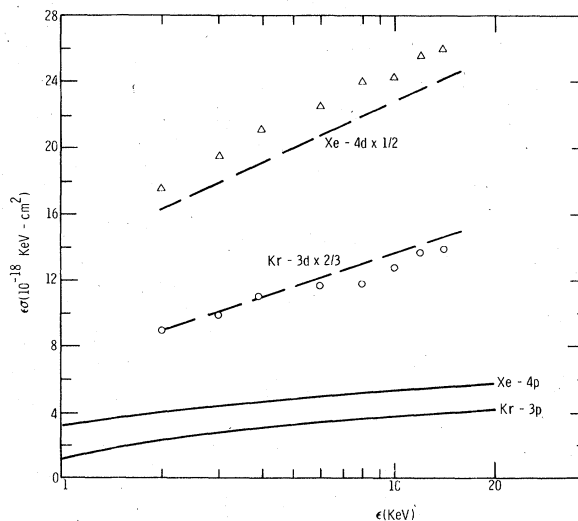


FIG. 7. Bethe plot of the ionization cross section for the  $3p(4p)$  subshell of Kr (Xe). The circles (Kr) and triangles (Xe) are measurements from Ref. 21 of the cross section for producing triply charged ions. The dashed lines are  $d$  subshell plots from Fig. 6 reduced by  $\frac{1}{3}$  (Kr) and  $\frac{1}{2}$  (Xe).

inately decay via a Coster-Kronig transition to  $(3d)^9(4s)^2(4p)^5 [(4d)^9(5s)^2(5p)^5]$  or  $(3d)^9(4s)^1(4p)^6 [(4d)^9(5s)^1(5p)^6]$ . Larkin's calculations<sup>22</sup> indicate that it is energetically possible for the doubly charged ions with a  $d$  hole to Auger decay to the triply charged ion. Thus we assume doubly charged ions are entirely due to  $d$ -shell holes.

In Fig. 6 the calculations are compared to the measurements of El-Sherbini *et al.* For the Kr  $3d$  subshell there is remarkable agreement, and for the Xe  $4d$  subshell, agreement to 20%, with the theory higher than the measurements. This agreement is puzzling in light of the disagreement in cross sections for singly charged ions and the agreement for total cross section. The puzzle is resolved if we examine the cross sections for producing higher stages of ionization. Using the above argument, we expect the cross section for production of triply charged ions to be dominated by the  $3p(4p)$  cross section in Kr (Xe). Comparison with the data of El-Sherbini *et al.* in Fig. 7 indicates a substantial disagreement both in magnitude and slope. In Fig. 8 the sum of the cross sections for producing ions with charge +4, +5, and +6 is compared with the calculated residual cross sections ( $\sum_{nl=1s}^{3s} \sigma_{nl}$  for Kr and  $\sum_{nl=1s}^{4s} \sigma_{nl}$  for Xe). In Fig. 8 the calculations and experiment differ in magnitude, but are comparable in slope. Thus the measurements of Ref. 21 show that there is a shift of GOS from the outer  $p$  shell to the inner shells.

The surprising feature in the comparison of the calculations and experiment is the good agreement

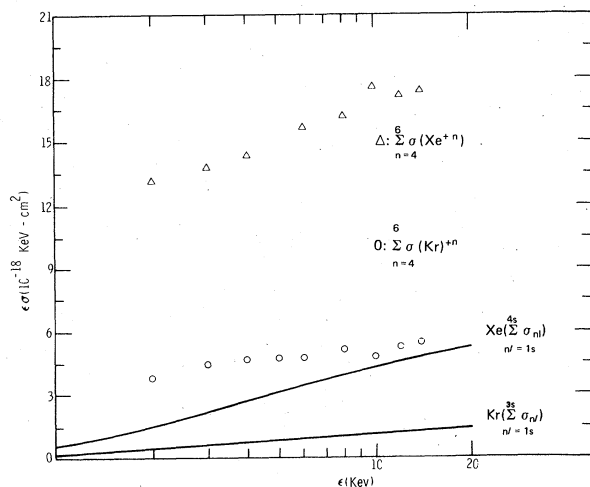


FIG. 8. Bethe plot for producing ions with charge greater than 3. For Kr (Xe) the calculated cross section is summed from 1s to 3s (4s). The measurements from Ref. 21 include only ions with charge +4, +5, and +6.

in the total cross section. Since the calculated cross section depends on the integral of GOS divided by energy, and since one knows from photoionization calculations<sup>8,23</sup> that the one-electron Herman-Skillman calculations lead to poor optical oscillator strengths (too high at threshold and dropping off too rapidly with increasing photon energy) for the outer shells of Kr and Xe, one expects an overestimate of the outer *p*-subshell ionization cross section. However, from Fig. 1, experimentally one finds additional outer-subshell oscillator strength at high energy. This region of GOS would lead to an underestimate of the calculated outer-subshell cross sections. From the latter consideration, it is not apparent that the calculated outer *p*-subshell cross section will be lower or higher than the measurement. Further, considerations of the distribution in energy of individual subshell GOS cannot account for the shift of GOS from outer subshells to inner subshells. This can occur due to configuration interaction involving configurations which Auger decay to higher stages of ionization than do the single inner-shell holes. An indication that this occurs is seen when the Bethe plots for the outer *d* electrons in Fig. 6 are redrawn in Fig. 7 multiplied by a factor of  $\frac{2}{3}$  for Kr and  $\frac{1}{2}$  for Xe. These are the dashed curves in Fig. 7. These Bethe plots agree in slope with the measurements. The 3*d* ionization threshold in Kr (93.8 eV)<sup>24</sup> is higher than the energy required to produce Kr<sup>+3</sup>, (75.5 eV),<sup>20</sup> and the 4*d* ionization threshold in Xe (67.6 eV)<sup>24</sup> is higher than the energy required to produce Xe<sup>+3</sup> (65.4 eV).<sup>20</sup> However, I have elsewhere<sup>25</sup> shown that the calcu-

lated  $M_{4,5} NN$  Auger spectrum of Kr is in good agreement with the measurements,<sup>26,27</sup> and the two-hole vacancy states  $(4s)^0(4p)^6$  and  $(4s)^1(4p)^5$  lie below the Kr<sup>+3</sup> ionization threshold. Thus the production of triply charged ions via ionization of the outer *d* subshell must occur via configuration interaction.

#### IV. ALKALIS AND ALKALI EARTHS

In Fig. 9 the calculated electron total ionization cross sections of K and Rb are compared with the measured values of MacFarland and Kinney<sup>28</sup> (open circles and triangles). The measurements are larger than the calculations. A similar disagreement was found<sup>1</sup> for Li and Na, and I suggested that the Li and Na data should be renormalized. Later measurements by Jalin *et al.*<sup>29</sup> confirmed a factor-of-2 error in the measurements of MacFarland and Kinney on Li. Thus, in Fig. 9, the filled circles and triangles are the K measurements multiplied by 0.41, and the Rb measurements multiplied by 0.83, respectively, to normalize the measurements to the calculations at 500 eV.

In discussing the alkali earths, I begin with Mg. The calculations and three sets of measurements are shown in Fig. 10. The recent measurements of Karstensen and Schneider,<sup>30</sup> shown as open squares, are in excellent agreement with the calculations between 30 and 60 eV. The data of Vainshtein *et al.*<sup>31</sup> agree with that of Karstensen and

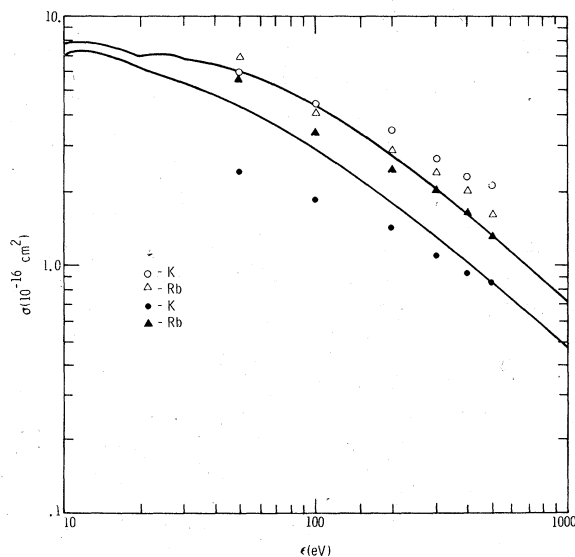


FIG. 9. Electron ionization cross section of K and Rb. The open circles (K) and open triangles (Rb) are from Ref. 28. The solid circles and triangles are the measured values for K and Rb, multiplied by 0.41 and 0.83, respectively (normalized to the calculation at 500 eV).

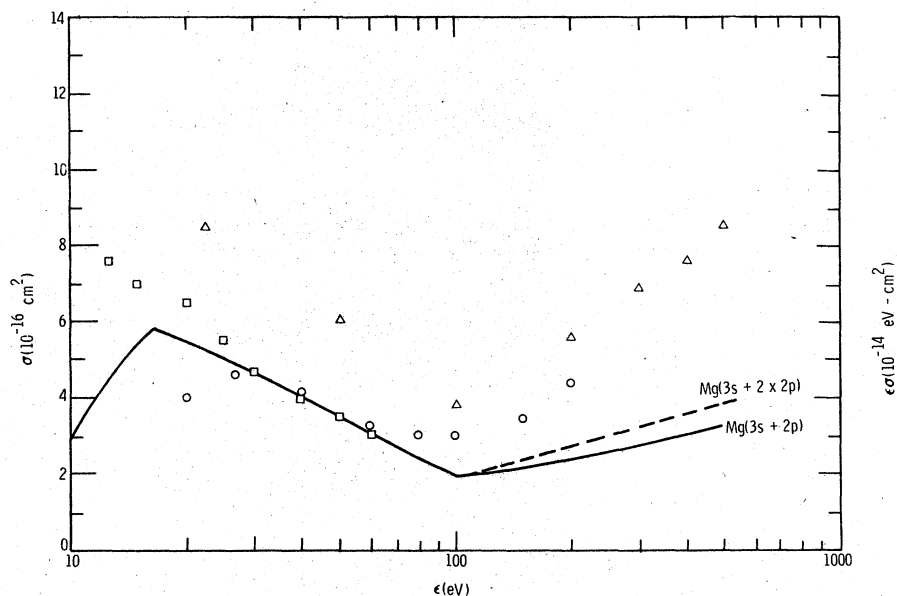


FIG. 10. Electron ionization cross section of Mg; above 100 eV the results are presented in a Bethe plot. The squares, circles, and triangles are from Refs. 30, 31, and 32, respectively.

Schneider<sup>30</sup> (and the calculations) between 30 and 60 eV, but the data of Vainshtein<sup>31</sup> *et al.* are considerably lower than that of Karstensen and Schneider<sup>30</sup> at low energy, and considerably larger than the calculations at high energies. Above 100 eV the results are shown as  $E\sigma(E)$  vs  $E$  for clarity. The measurements of Okuno *et al.*<sup>32</sup> are larger than those of Vainshtein *et al.*<sup>31</sup> at high energies, and both are larger than the calculations. The agreement between the calculation and two sets of measurements between 30 and 60 eV indicates agreement for the Mg 3s ionization cross section. The disagreement between calculation and experiment at higher energies could arise from a poor calculation of 2p ionization. However at 500 eV Okudaira *et al.*<sup>33</sup> measure the ratio of doubly charged to singly charged ions as 0.38 while my calculated ratio is 0.40. Further, the calculated electron ionization cross section of Ne<sup>1</sup> was in excellent agreement with measured values, and it is unreasonable to expect the calculated 2p cross section to become poorer as one goes to higher  $Z$ . Finally, the measurements of Okuno *et al.* are roughly a factor-of-2 higher than Peach's<sup>10</sup> calculations at high energy. The conclusion I reach from this comparison of calculation and measurement on Mg is that there is a possibility of error in the measurements.

The comparison for Mg was discussed in detail because comparable discrepancies exist for Ca and Sr, shown in Fig. 11. The measurements are those of Vainshtein *et al.*<sup>31</sup> and Okuno.<sup>34</sup> For Ca and Sr, unlike Mg, the two sets of measurements agree above 100 eV. However, the data on Ca and Sr disagree with the calculations above 50 eV, in

a fashion similar to the data of Vainshtein *et al.*<sup>31</sup> on Mg above 80 eV. Both Fayard *et al.*<sup>35</sup> and Okudaira<sup>36</sup> have measured the ratio of double-to-single ion production at 500 eV in Ca. The former find a ratio of 0.72 and the latter finds 0.94. I calculate  $(\sigma_{3s} + \sigma_{3p})/\sigma_{4s} = 0.49$ . Ziesel<sup>37</sup> and Okudaira<sup>36</sup> have measured the double-to-single-ion ratio at 500 eV in Sr. The former finds 0.56 and the latter 1.10. I calculate  $(\sigma_{4s} + \sigma_{4p})/\sigma_{5s} = 0.72$ . If the measurements of Okudaira<sup>36</sup> are valid (other measurements are significantly lower), and one attributes the difference between the calculations and measurements to an underestimate of the  $(\sigma_{3s} + \sigma_{3p})$  in Ca and  $(\sigma_{4s} + \sigma_{4p})$  in Sr, then renormalizing the calculations to Okudaira's<sup>36</sup> measured ratio would bring the calculation closer to, but still below the measurements of Okuno.<sup>34</sup> However, for Ar my calculated  $(\sigma_{3s} + \sigma_{3p})$  is in good agreement with the measurements,<sup>1</sup> and in Kr the calculated  $(\sigma_{4s} + \sigma_{4p})$  is higher than the measurements. It is not clear why the calculations should underestimate the summed cross sections when  $Z$  is increased by two units.

## V. ASSORTED OTHER ELEMENTS

Silver is widely used for calibration in high-temperature mass spectrometry. We have not calculated the Ag electron ionization cross section, but have done so for Pd, Cd, and Sn with  $Z = 46, 48,$  and  $50,$  respectively. There are two sets of measurements on Ag, by Crawford and Wang,<sup>38</sup> and by Pavlov *et al.*<sup>39</sup> They differ by 40%. The calculations and data are shown in Fig. 12. For Pd the total cross section is dominated by 4d-subshell ionization, and we neglect inner-shell

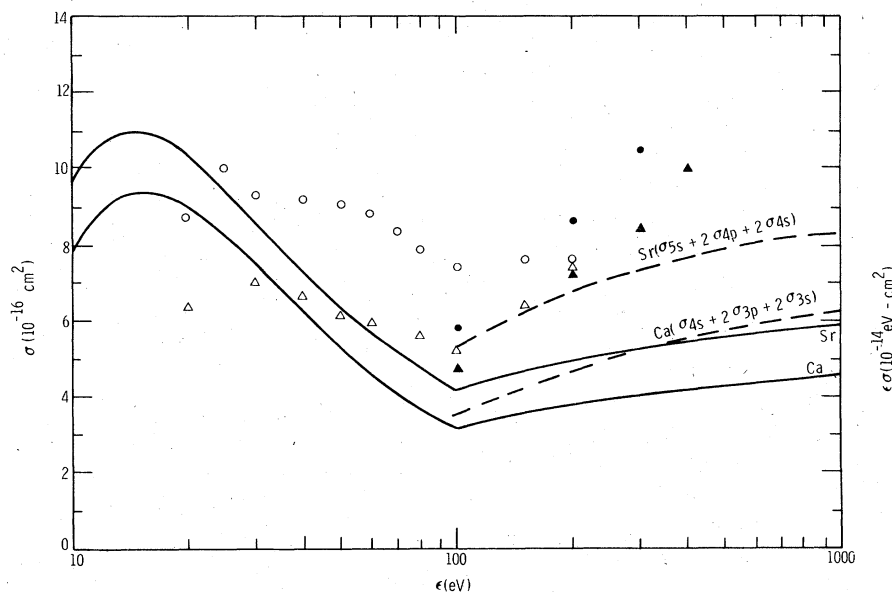


FIG. 11. Electron ionization cross section of Ca and Sr; above 100 eV the results are presented in a Bethe plot. The open triangles (Ca) and circles (Sr) are from Ref. 31; the closed triangles (Ca) and circles (Sr) are from Ref. 34.

ionization followed by Auger decay, which leads to multiply charged ions and an enhanced cross section. For Ag, with a single electron outside the  $4d$  shell, this neglect is valid. However, for Cd and Sn, Auger decay of the  $4d$  shell is important, and so we show the Cd and Sn results, both with (dashed curves) and without (solid curves) Auger decay of the  $4d$  hole. Lin and Stafford<sup>40</sup> have measured Sn/Ag and Ge/Ag cross-section ratios at 60 eV to be  $1.46 \pm 0.16$  and  $1.46 \pm 0.3$ , respectively. From the Sn calculation in Fig. 12 and the Ge calculation in Fig. 13 the Ag cross sec-

tion is  $5.83 \pm 0.6 \text{ \AA}^2$ , and  $5.42 \pm 1.15 \text{ \AA}^2$ , respectively. Mann<sup>41</sup> estimates a value for the Ag cross section at maximum of  $5.44 \text{ \AA}^2$ , consistent with the measurements of Lin and Stafford<sup>40</sup> and our Sn and Ge cross sections. The value measured by Crawford and Wang<sup>38</sup> is  $4.6 \text{ \AA}^2$ , and, by itself, is consistent with the Sn/Ag and Ge/Ag ratios, if it is assumed that the calculated Sn and Ge cross sections are somewhat too large at 60 eV. However, both the measurements of Crawford and Wang<sup>38</sup> and Pavlov *et al.*<sup>39</sup> are lower than the calculations at high energy. When Auger decay of

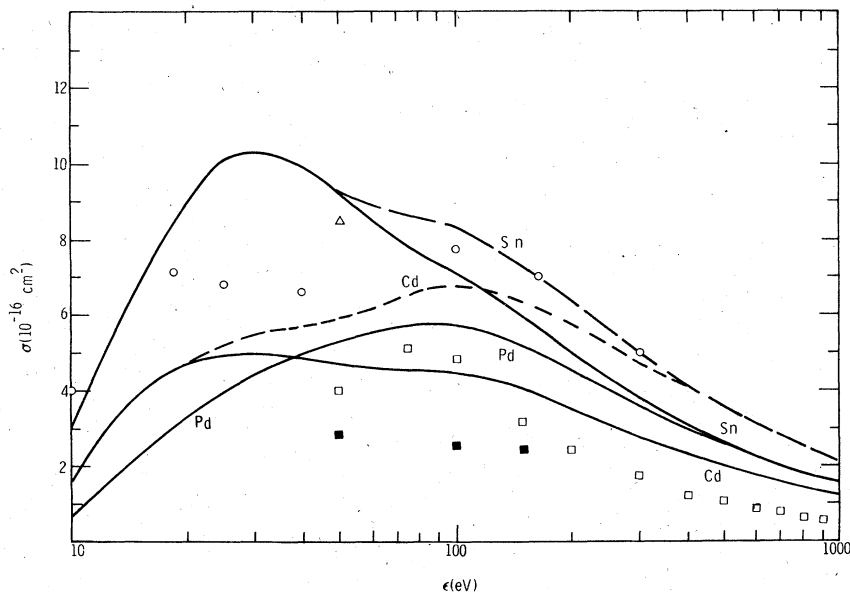


FIG. 12. The solid curves are the calculated electron ionization cross sections of Pd, Cd, and Sn. The dashed curves correct the Cd and Sn results for double ion production. The open and solid squares are measurements on Ag from Refs. 38 and 39, respectively. The open circles are measurements from Ref. 42, while the open triangle is a Cd measurement from Ref. 43.

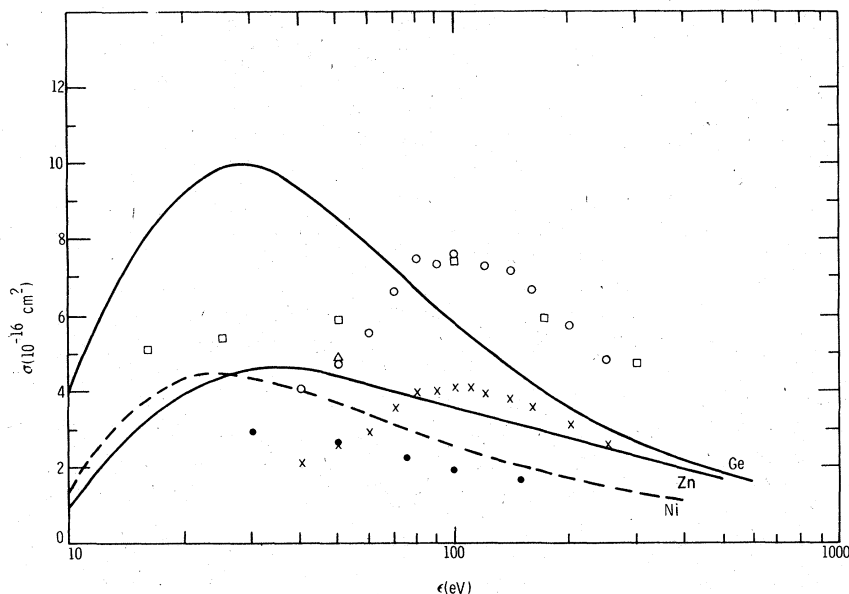


FIG. 13. The solid curves are the calculated electron ionization cross sections of Ni, Zn, and Ge. The solid circles, open circles, and crosses are Cu measurements of Refs. 39, 44, and 45, respectively. The open squares are measurements on Ga from Ref. 42, while the open triangle is a Zn measurement from Ref. 43.

the  $4d$  shell is included, the total ionization cross sections for Cd and Sn are almost identical at high energy. Shimon *et al.*<sup>42</sup> have measured the total ionization cross section of the intervening element In ( $Z=49$ ) and their results lie between the dashed curves for Cd and Sn. While the agreement is gratifying, some skepticism is warranted. Shimon *et al.*<sup>42</sup> also measure similar bumps in the total ionization cross section of Ga and Al at 100 eV, while for Al the calculations indicate no bump. Pottie<sup>43</sup> has measured the Cd ionization cross section at 50 eV, and it is 40% larger than the calculation.

For electron ionization of Cu, there are three sets of measurements, all in disagreement. Those of Schroerer *et al.*<sup>44</sup> are a factor of 1.85 larger than those of Crawford,<sup>45</sup> though they agree in shape. Those of Pavlov *et al.*<sup>39</sup> differ both in magnitude and shape from the other two sets. In Fig. 13, we show the measurements and the total ionization cross section for Ni ( $Z=28$ ) and Ge ( $Z=32$ ). For Zn ( $Z=30$ ) we show  $\sigma_{4s} + 2\sigma_{3d}$ . For Zn, we assume  $3d$ -subshell ionization leads to doubly charged ions. For Ni, we assumed a configuration  $(3d)^9(4s)$ , so no Auger decay follows  $3d$ -subshell ionization. For Ge the  $3d$ -ionization cross section is less than 20% of the total even at 1 keV, and we did not correct the calculation for doubly charged ions. The calculations clearly support the measurements of Crawford.<sup>45</sup> Pottie<sup>43</sup> has measured the electron ionization cross section of Zn at 50 eV. His value,  $5.0 \text{ \AA}^2$ , is consistent with the calculation. Shimon *et al.*<sup>42</sup> have measured the electron ionization cross section of Ga ( $Z=31$ ). Their results are similar to their measurements on In,

showing a peak at 100 eV, where the calculations show no peak. With the scaled cross sections it will be possible to make a stronger statement. However, in the same series of experiments Shimon *et al.*<sup>42</sup> measured the electron ionization cross section of Al. A comparison of their measurements with the present calculations is made in Fig. 14. For Al, I show the calculated  $3s + 3p$  electron ionization cross section. My calculated  $2p$ -ionization cross section has a maximum cross section of  $0.1 \text{ \AA}^2$ , thus  $2p$ -ionization followed by Auger decay will increase the calculations by no more than  $0.2 \text{ \AA}^2$ . Thus relative to the calculations on Al, the data of Shimon *et al.*<sup>42</sup> shows an unexpected peak at 100 eV. It is possible that the difference lies in the normalization of the data as in the difference between the measurements on Cu of Schroerer *et al.*<sup>44</sup> and Crawford.<sup>45</sup> However, the difference between

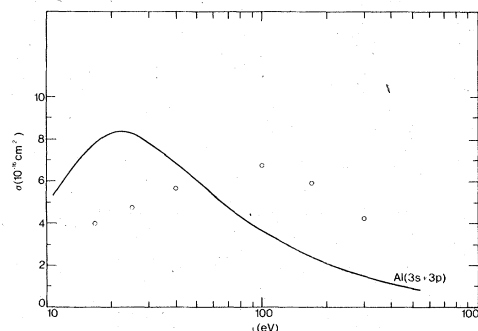


FIG. 14. Electron ionization cross section of Al. The solid line is the sum of the  $3s$  and  $3p$  cross sections. The open circles are measurements from Ref. 42.

calculation and experiment in Fig. 14 is similar to the discrepancies seen in the alkali earths.

## VI. CONCLUSIONS

Calculations were made for the electron ionization cross section for 20 elements with  $19 \leq Z \leq 54$ . Comparison with measurements of the total ionization cross section for Kr and Xe showed good agreement above 300 eV. However, a detailed comparison of the subshell cross sections with measurements of the cross sections for producing various charge states in Kr and Xe showed significant discrepancies. The discrepancies are consistent with a description of inner-shell vacancies involving substantial configuration interaction, i.e., a breakdown in the one-electron description. However, one-electron ionization cross-section cal-

culations can still be useful if the subshell cross sections scale in a simple fashion, because ionization in the Born approximation involves a one-electron operator. To use the scaled cross sections then requires knowledge of the relevant interacting configurations, their energies, and configuration mixing parameters. Since total cross sections are obtained via ion current measurements, which measure total electron production (secondary plus Auger), the agreement between calculation and measurement for Kr and Xe indicates that the Born approximation is reliable for estimating such processes. However, for almost all the other elements for which comparison with calculations could be made, there were significant discrepancies. The comparison for Cu indicates that the experimental procedure may be the cause of some of the discrepancies.

\*Work supported by the U. S. Energy Research and Development Administration.

<sup>1</sup>E. J. McGuire, Phys. Rev. A **3**, 267 (1971).

<sup>2</sup>E. J. McGuire, J. Phys. (Paris), Colloq. **10** **32**, C4-37 (1971).

<sup>3</sup>A. E. S. Green, D. L. Sellin, and A. S. Zacher, Phys. Rev. **184**, 1 (1969); P. S. Ganas and A. E. S. Green, Phys. Rev. A **4**, 182 (1971); P. A. Kazaks, P. S. Ganas, and A. E. S. Green, Phys. Rev. A **6**, 2169 (1972).

<sup>4</sup>K. Omidvar, H. L. Kyle, and E. C. Sullivan, Phys. Rev. A **5**, 1174 (1972).

<sup>5</sup>S. T. Manson, Phys. Rev. A **5**, 668 (1972); **6**, 1013 (1972).

<sup>6</sup>W. Lotz, Z. Phys. **206**, 205 (1967); **232**, 101 (1970).

<sup>7</sup>F. Herman and S. Skillman, *Atomic Structure Calculations* (Prentice-Hall, Englewood Cliffs, N. J., 1963).

<sup>8</sup>E. J. McGuire, Phys. Rev. **175**, 20 (1968).

<sup>9</sup>H. Bethe, Ann. Phys. (Leipzig) **5**, 325 (1930).

<sup>10</sup>G. Peach, Proc. Phys. Soc. Lond. **85**, 709 (1965); **85**, 375 (1966); J. Phys. B **1**, 1088 (1968).

<sup>11</sup>E. J. McGuire, Phys. Rev. A **14**, 1576 (1976).

<sup>12</sup>D. J. Kennedy and S. T. Manson, Phys. Rev. A **5**, 227 (1972).

<sup>13</sup>J. B. West, P. R. Woodruff, K. Codling, and R. G. Houlgate, J. Phys. B **9**, 407 (1976).

<sup>14</sup>M. Y. Amusia, in *Proceedings of the Fourth International Conference on VUV Radiation Physics, Hamburg*, edited by E. E. Koch, R. Haensel, and C. Kunz (Pergamon, Braunschweig, 1974).

<sup>15</sup>U. Gelius, J. Electron Spectros. and Relat. Phenom. **5**, 985 (1974).

<sup>16</sup>D. Rapp and P. Englander-Golden, J. Chem. Phys. **43**, 1465 (1965).

<sup>17</sup>R. K. Asundi and M. V. Kurepa, J. Electron. Control. **15**, 41 (1963).

<sup>18</sup>B. L. Schram, F. J. DeHeer, M. J. Van Der Wiel, and J. Kistemaker, Physica **31**, 94 (1965).

<sup>19</sup>B. F. Luyken, F. J. DeHeer, and R. Ch. Baas, Physica **61**, 200 (1972).

<sup>20</sup>C. E. Moore, *Atomic Energy Levels*, Natl. Bur. Stds. (U.S.) Circ. No. 467 (U.S. GPO, Washington, D.C., 1957).

<sup>21</sup>Th. M. El-Sherbini, M. J. Van Der Wiel, and F. J. DeHeer, Physica **48**, 159 (1970).

<sup>22</sup>F. P. Larkins, J. Phys. B **6**, 2450 (1973).

<sup>23</sup>J. W. Cooper, Phys. Rev. **128**, 681 (1962).

<sup>24</sup>K. Codling and R. P. Madden, Phys. Rev. Lett. **12**, 106 (1964).

<sup>25</sup>E. J. McGuire, Phys. Rev. A **11**, 17 (1975).

<sup>26</sup>L. O. Werme, T. Bergmark, and K. Siegbahn, Phys. Scr. **6**, 141 (1972).

<sup>27</sup>W. Mehlhorn, W. Schmitz, and D. Stalherm, Z. Phys. **252**, 399 (1972).

<sup>28</sup>R. H. MacFarland and J. D. Kinney, Phys. Rev. A **137**, 1058 (1956).

<sup>29</sup>R. Jalin, R. Hagemann, and R. Botter, J. Chem. Phys. **59**, 952 (1973).

<sup>30</sup>F. Karstensen and M. Schneider, Z. Phys. A **273**, 321 (1975).

<sup>31</sup>L. A. Vainshtein, V. I. Ochkur, V. I. Rakhovskii, and A. M. Stepanov, Zh. Eksp. Teor. Fiz. **61**, 511 (1971) [Sov. Phys.-JETP **34**, 271 (1972)].

<sup>32</sup>Y. Okuno, K. Okuno, Y. Kaneko, and I. Kanomata, J. Phys. Soc. Jpn. **29**, 164 (1970).

<sup>33</sup>S. Okudaira, Y. Kaneko, and I. Kanomata, J. Phys. Soc. Jpn. **28**, 1536 (1970).

<sup>34</sup>Y. Okuno, J. Phys. Soc. Jpn. **31**, 1189 (1971).

<sup>35</sup>F. Figuet-Fayard and M. Lahmani, J. Chim. Phys. **59**, 1050 (1962).

<sup>36</sup>S. Okudaira, J. Phys. Soc. Jpn. **29**, 409 (1970).

<sup>37</sup>J. P. Ziesel, J. Chim. Phys. **64**, 706 (1967).

<sup>38</sup>C. K. Crawford and K. I. Wang, J. Chem. Phys. **47**, 4667 (1967).

<sup>39</sup>S. I. Pavlov, V. I. Rakhovskii, and G. M. Fedorova, Zh. Eksp. Teor. Fiz. **52**, 21 (1967) [Sov. Phys.-JETP **25**, 12 (1967)].

<sup>40</sup>S. S. Lin and F. E. Stafford, J. Chem. Phys. **47**, 4664 (1967).

<sup>41</sup>J. B. Mann, J. Chem. Phys. **46**, 1646 (1967).

<sup>42</sup>L. L. Shimon, E. I. Nepitipov, and I. P. Zapesochnyi, Zh. Tekh. Fiz. **45**, 688 (1975) [Sov. Phys.-Tech. Phys. **20**, 434 (1975)].

<sup>43</sup>R. F. Pottie, J. Chem. Phys. **44**, 916 (1966).

<sup>44</sup>J. M. Schroeder, D. H. Gündüz, and S. Livingston, J. Chem. Phys. **58**, 5135 (1973).

<sup>45</sup>C. K. Crawford, Tech Rept. No. 1, Particle Optics Laboratory, MIT, Cambridge, Mass., 1969, AFML-TR-67-376 (unpublished).